https://doi.org/10.20965/ijat.2023.p0434

Research Paper:

Effect of Vibration Behavior in Low-Frequency Vibration Cutting on Surface Properties of Workpiece

Hiroyuki Kodama†, Shota Matsuno, Naoyuki Shibata, and Kazuhito Ohashi

Okayama University
3-1-1 Tsushima Naka, Okayama 700-8530, Japan
†Corresponding author, E-mail: h-kodama@okayama-u.ac.jp
[Received January 31, 2023; accepted May 24, 2023]

The objective of this study was to determine the effect of vibration behavior on workpiece surface properties in low-frequency vibration cutting. The effects of the parameters that determine vibration behavior on surface roughness were quantitatively evaluated through a comparison with other cutting conditions. Furthermore, by clarifying how the surface properties of the workpiece, such as roughness, roundness, and cross-sectional curves, change depending on the vibration behavior, a search for optimal conditions for low-frequency vibration cutting was conducted. The best surface properties were obtained under the condition of spindle rotation per vibration $E = 4.5$. By using a value close to the minimum possible spindle rotation $R = 0.5$ when the workpiece is retracted, it is expected to be effective in suppressing the variation in surface roughness at each phase angle; this variation is characteristic of low-frequency vibration cutting. Workpieces machined under low-frequency vibration conditions such as ($E = 2.5$, $R = 1.0$) and ($E = 3.5$, $R = 1.0$) were found to form characteristic surface patterns on the workpiece surface owing to a phenomenon in which the depth of the cut to the workpiece changes.

Keywords: low-frequency vibration cutting, vibration behavior, surface roughness, cross-sectional curve

1. Introduction

Continuous cutting, including turning, is widely used in the machining of many parts [1], and research is still being conducted to realize high-speed, high-efficiency, and high-precision continuous cutting [2]. However, the chips ejected by continuous cutting can become entangled in the workpiece, tools, and machine tools, resulting in operating losses due to incidental work for chip removal [3]. These operations decrease productivity and are obstacles to fully automated and unmanned continuous cutting [4]. In continuous cutting, the workpiece and tool are always in contact, which increases the contact pressure between the tool and chips [5]. Furthermore, in general-purpose turning, supplying cutting fluid to the cutting point is difficult; therefore, the thermal and mechanical loads on the tool are greater than those during intermittent cutting [6, 7]. Vibration cutting, in which vibration is applied to the tool to perform machining, has been studied in recent years as a solution to the abovementioned problems in continuous cutting. In the past, ultrasonic and elliptical vibrations have been used in vibration cutting, and shakers such as piezoelectric devices have been mainly used for vibration excitation [8]. However, conventional methods have drawbacks in terms of vibration control and restrictions on machining geometry due to the need for additional equipment, and they are unable to handle various types of turning operations, such as taper, arc, and drilling operations.

In recent years, the chip-breaking effect of low-frequency vibration cutting has made it possible to reduce the aforementioned operating loss. Low-frequency vibration cutting is a method of cutting that numerically controls the workpiece to vibrate in the cutting feed direction while synchronizing the vibration with the spindle rotation; by adding idle time during cutting, it is possible to machine while breaking chips into small pieces [9].

Generally, there are three low-frequency vibration cutting modes that match the machining task: Modes 1, 2, and 3 [10]. **Fig. 1** shows the characteristics of each mode and the cutting edge trajectory model. Mode 1 is suitable for machining difficult-to-machine materials, and sets the number of vibration cycles per workpiece rotation to break up the chips into small pieces [5]. Mode 2 sets the number of workpiece rotations per vibration when peripheral speed is required, such as in the machining of fine workpieces and small-diameter deep holes. Therefore, it is characterized by a coarser chip breakup than mode 1. Mode 3 is used to break up chips during threading. More research results have been reported on low-frequency vibration cutting using mode 1 than using mode 2 [11]. In addition, the machining surface creation mechanism of low-frequency vibration cutting and its effect on surface shapes have been clarified. Furthermore, the optimum values of feed rate f and vibration amplitude ratio Q, which are the conditions for low-frequency vibration cutting in mode 1, have been clarified, and it has been confirmed that the characteristic unevenness of the contour shape, which has been an issue in low-frequency vibration cutting, is suppressed [11, 12]. However, little is

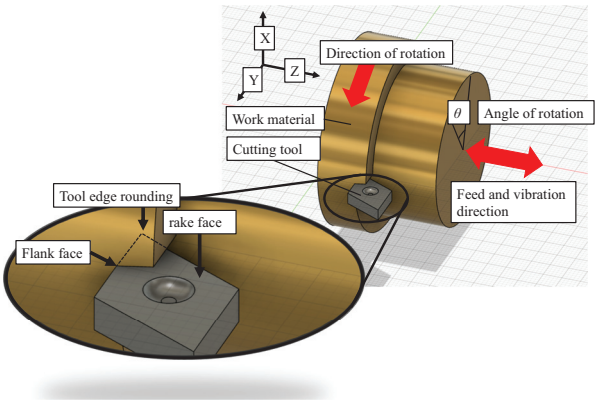

(a) Schematic diagram of low frequency vibration cutting.

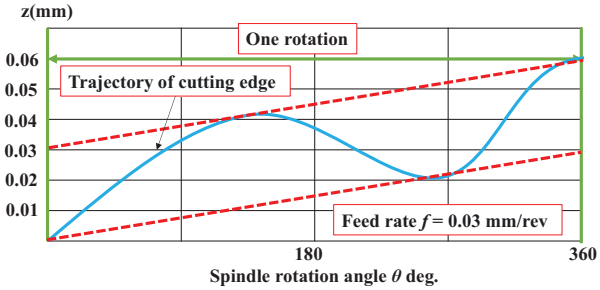

(b) Low-frequency vibration behavior of mode 1: The number of vibrations per workpiece rotation is specified. Chips are broken into smaller pieces.

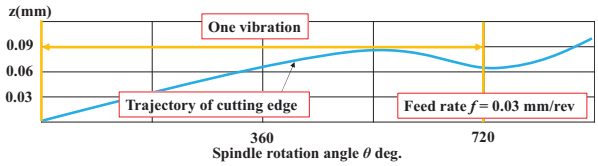

(c) Low-frequency vibration behavior of mode 2: The number of rotations per vibration is specified. The machining speed is faster than that in mode 1 because machining can be performed under conditions with less vibration. This mode is suitable for machining that requires peripheral speed, such as small-diameter work material machining and small-diameter deep hole machining.

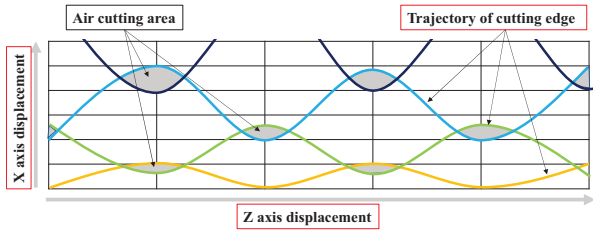

(d) Low-frequency vibration behavior of mode 3: The vibration timing is changed for each threading pass. By vibrating in the cutting direction, chips are broken during thread cutting.

Fig. 1. Vibration behavior and characteristics in each mode.

known about the effects of vibration behavior on the cutting resistance, tool load, and surface finish of the cut surface, in addition to the effect of improved chip removal in low-frequency vibration cutting technology using mode 2. In particular, it has been reported that the characteristics of low-frequency vibration cutting vary depending on the vibration behavior [13]. However, experimental verification of the effects of different vibration behaviors on the cutting characteristics and changes in workpiece surface properties is lacking. The low-frequency vibration conditions for mode 2, which differ from those for mode 1, are the spindle rotation per vibration E and the spindle rotation when the workpiece is retracted R. The effects of the above differences in vibration behavior on the changes in cutting characteristics have not been experimentally verified. In addition, at production sites where the production of many different products in small quantities is required, a reduction in the cycle time is always being sought [13].

The objective of this study was to clarify how the vibration behavior in mode 2 of low-frequency vibration cutting affects the surface properties of the workpiece, as a higher feed rate and cutting speed can be set in this mode. In addition to examining the effects of different vibration behaviors on the surface roughness and cross-sectional profile, the optimal vibration conditions were investigated. Moreover, when discussing the machinability of the processed materials, many factors affect the cutting conditions in a complex manner [14]. Therefore, the optimum vibration conditions were derived by evaluating the surface properties of the workpiece under a large number of low-frequency vibration conditions and examining the detailed surface roughness transitions and their relationship to the vibration behavior. Furthermore, the mechanism of regular cross-sectional curve formation in low-frequency vibration cutting, cutting resistance, and changes in the effect of vibration behavior on surface properties due to differences in tool geometry were also investigated.

2. Characteristics of Low-Frequency Vibration Cutting

2.1. Vibration Behavior Control by Low-Frequency Vibration Parameters

In low-frequency vibration cutting using mode 2, the feed of the spindle is controlled such that the feed rate when moving in the $+Z$ direction is equal to that when moving in the $-Z$ direction. Therefore, the feed changes depending on the combination of the set feed rate and arguments E and R. **Table 1** lists the feed per spindle rotation for each condition. This indicates that as argument E increases, the effect of spindle retraction is relatively small and the feed rate approaches that of conventional cutting. As argument R increases, the displacement in the Z direction in one vibration is fixed and is therefore greatly affected by spindle retraction, resulting in a larger feed. Under the conditions of $E = 4.5$ and $R = 0.5$, the feed per rotation was the smallest (0.058 mm), whereas when $E = 2.0$ and $R = 1.0$, the feed per rotation was the largest at 0.135 mm. This value was three times that of the feed rate setting $f = 0.045$ mm/rev.

Here, we explain arguments E and R as parameters for controlling low-frequency vibration using mode 2. E

Table 1. Feed width per spindle revolution under each condition.

(Unit : mm/rev)

E argument \ *R* argument	0.5	0.6	0.7	0.8	0.9	1.0
2.0	0.090	0.096	0.104	0.113	0.123	0.135
2.5	0.075	0.079	0.083	0.088	0.094	0.100
3.0	0.068	0.070	0.073	0.077	0.080	0.084
3.5	0.063	0.065	0.068	0.070	0.073	0.076
4.0	0.060	0.062	0.064	0.066	0.068	0.070
4.5	0.058	0.059	0.061	0.063	0.064	0.066

represents the spindle rotation per vibration and R represents the spindle rotation when the workpiece is retracted. **Fig. 2** shows examples of the three vibration behavior patterns during low-frequency vibration cutting. The shaded area indicates the idle zone, where the tool and workpiece do not interfere during cutting, which enables machining while intermittently breaking up chips.

Figure 2(a) shows the low-frequency vibration behavior at a set feed rate of $f = 0.03$ mm/rev, $E = 2.0$, and $R = 1.0$. Because the feed rate is 0.03 mm/rev, the feed trajectory during conventional cutting is as shown by the gray dotted line. The feed trajectory during low-frequency vibration cutting is displaced in the $+Z$ direction at the first rotation and in the $-Z$ direction at the second rotation, as shown in **Fig. 2**. Similarly, the displacement at the third rotation is in the $+Z$ direction, and that at the fourth rotation is in the $-Z$ direction. In this manner, cutting is performed while repeating the displacement behavior in the $+Z$ direction for one rotation and then in the $-Z$ direction for one rotation. The light blue area indicates the area to be cut when the workpiece is displaced in the $+Z$ direction, and the light red area indicates the area to be cut when the workpiece is displaced in the $-Z$ direction.

As shown in **Fig. 2(b)**, because the spindle rotation per vibration is 4.0 and the spindle rotation during retraction is 1.0, the displacement is in the $+Z$ direction from the first rotation, indicated by the blue line, to the third rotation, indicated by the yellow line, then the displacement switches to the $-Z$ direction at the fourth rotation, indicated by the red line. Next, from the fifth to seventh rotations, the displacement is in the $+Z$ direction, and in the eighth rotation, the displacement is in the $-Z$ direction. As in **Fig. 2(a)**, the light blue area indicates the area that is cut when the workpiece is displaced in the $+Z$ direction, and the light red area indicates the area that is cut when the workpiece is displaced in the $-Z$ direction.

In **Fig. 2(c)**, the spindle rotation per vibration is 2.0, as in **(a)**; however, the spindle rotation during retraction is 0.5, the vibration is displaced in the $+Z$ direction during the first rotation, and is then further displaced in the $+Z$ direction until the phase angle of 180° in the second rotation. The vibration behavior is repeated with displacement in the $-Z$ direction in the remaining half of the second rotation.

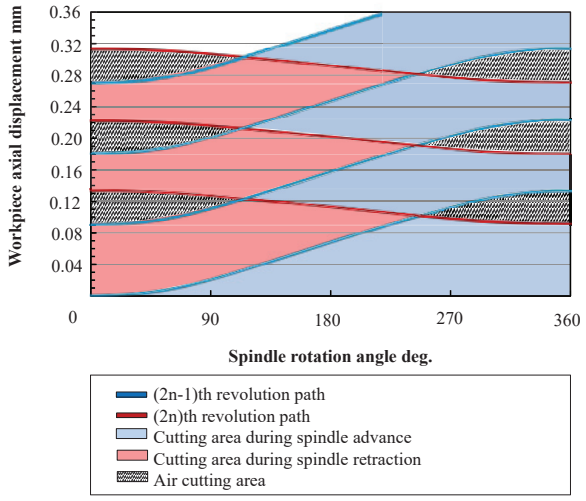

(a) $E = 2.0$, $R = 1.0$

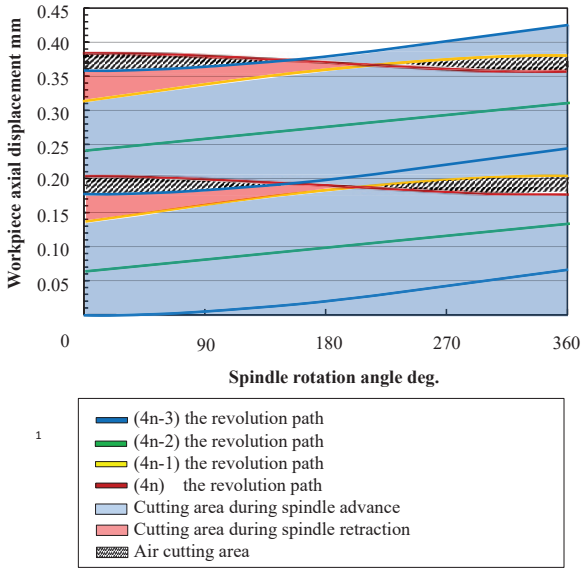

(b) $E = 4.0$, $R = 1.0$

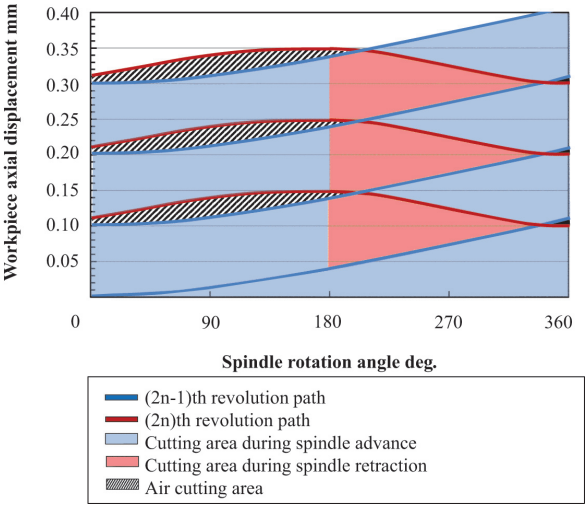

(c) $E = 2.0$, $R = 0.5$

Fig. 2. Low-frequency vibration behavior.

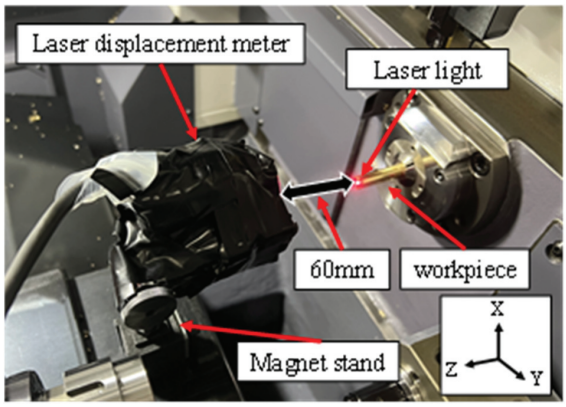

Fig. 3. Vibration behavior measurement method by using laser displacement meter.

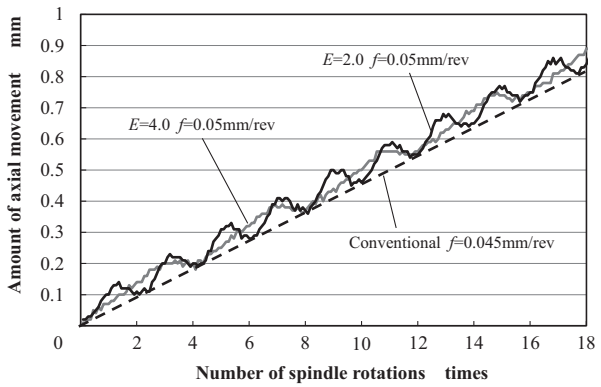

Fig. 4. Comparison of vibration behavior and conventional cutting.

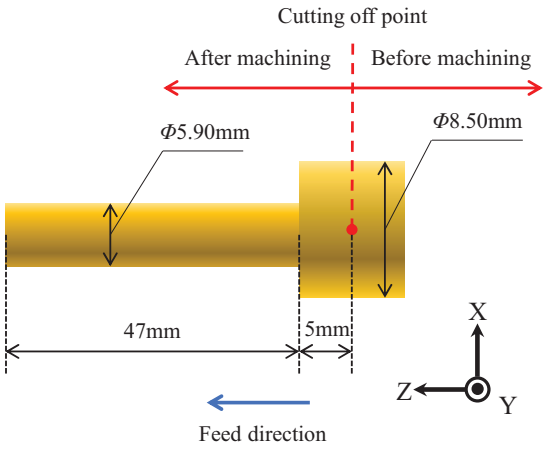

Fig. 5. Workpiece shape (before and after cutting).

In both cases, the machining cycle time was similar to that of conventional cutting. In **Figs. 2(a)** and **(c)**, the $+Z$-axis displacement of the workpiece after two rotations is similar, and in **Fig. 2(b)**, the $+Z$-axis displacement of the workpiece after four rotations is similar.

Compared to conventional cutting, the feed increases during low-frequency vibration cutting. As shown in the figure, the feed increases because the workpiece is displaced in the $-Z$ direction during machining, even though the machining cycle time is the same. Because the feed is controlled such that the feed rates when moving in the $+Z$ direction and when moving in the $-Z$ direction are equal when $R = 0.5$, it is determined by the combination of the set feed rate and arguments E and R.

2.2. Determination of Vibration Behavior and Maximum Feed Rate Using a Laser Displacement Meter

A laser displacement transducer (LK-G5000, LK-H050, Keyence) was used to determine the low-frequency vibration behavior in this experiment. **Fig. 3** shows the method for measuring vibration behavior using the laser displacement meter.

The laser displacement meter was fixed to a magnetic stand so that the laser beam irradiated the edge surface of the workpiece, and the low-frequency vibration behavior was measured by displacing the workpiece in the cutting feed direction while vibrating it at a low frequency. The distance between the laser displacement meter and the workpiece end face was 60 mm, even in the maximum range. Considering this measurement range and the characteristics of the machine tool, the vibration behavior was measured without actually cutting the workpiece.

In low-frequency vibration cutting, the servomotor is controlled by NC to vibrate the spindle; therefore, there is a limit to the frequency of vibration. The same is true for the feed rate. Therefore, we attempted to determine the maximum feed rate before conducting this experiment. **Fig. 4** shows the results of overlaying the low-frequency vibration behavior set at a feed rate of $f = 0.05$ mm/rev and the trajectory of conventional cutting at a feed rate of $f = 0.045$ mm/rev. For both the $E = 2.0$ and $E = 4.0$ conditions, the valley of the waveform, which is the end of each vibration, touches the black dashed line of the conventional cutting trajectory, indicating that the machining cycle time is the same in both methods. Therefore, the above results confirm that the maximum feed rate in low-frequency vibration cutting is $f = 0.045$ mm/rev.

3. Experimental Methods

3.1. Fundamental Experiments to Quantitatively Evaluate the Influence of Vibration Behavior on Workpiece Surface Properties

The workpiece material was free-cutting brass, JIS C3604, which has excellent cutting trace transferability [15]. C3604 is a cutting alloy in which Pb is added to brass [16] and is widely used for water valve materials and bearings because of its excellent free-cutting properties [17]. The material diameter, machining diameter, and workpiece length used in this experiment are shown in **Fig. 5**. **Fig. 6** shows the rake face geometry of the tool. A

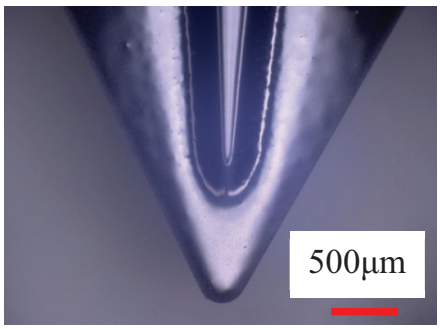

Fig. 6. Cutting edge shape.

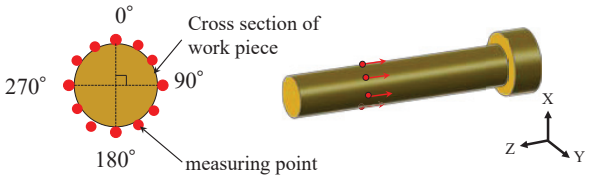

Fig. 7. Workpiece measurement method.

tool with a single layer of TiAlN coating and relatively high Al content manufactured by Mitsubishi Materials Corporation was used. The rake angle was 12°, relief angle was 7°, and tool edge roundness was $r = 0.18$ mm.

In this study, a CNC automatic lathe L12 equipped with a low-frequency vibration function, manufactured by Citizen Machinery, was used. This experimental machine presses a tool against a rotating workpiece for machining. The workpiece vibrates at a low frequency in the Z direction and is displaced in the positive direction while rotating to remove chips.

Figure 7 shows the workpiece measurement method. For each workpiece machined in this study, the surface roughness was measured at 12 points on the same circumference of one workpiece using a SURFCOM 1500DX2 stylus-type roughness meter (Tokyo Seimitsu). For workpieces machined by low-frequency vibration cutting, the starting point of measurement (0°) was defined as the point of displacement in the Z direction during machining, because different surface properties are formed depending on the phase angle of the workpiece.

In this experiment, cutting resistance was measured by using a strain gauge to investigate the cutting characteristics and machining phenomena during low-frequency vibration cutting. **Fig. 8** shows an overview of the experimental setup. A strain gauge was attached to the tool holder to enable the measurement of the main force and feed force during cutting. The strain gage is connected to a lead wire, which is connected to a bridge box, dynamic strain amplifier, and data logger to detect the main force and feed force as voltage values. Furthermore, cutting resistance was measured by converting the voltage values to load. As shown in **Fig. 8**, during low-frequency vibration cutting, the chips are removed while vibrating the workpiece in the cutting feed direction (Z direction).

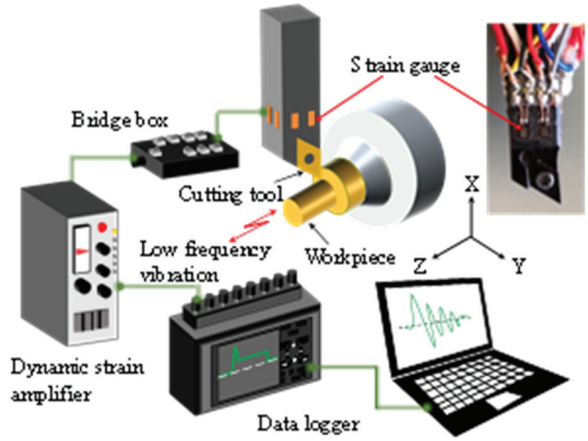

Fig. 8. Outline of experimental equipment.

Table 2. Cutting conditions.

Cutting machine	L12 by Citizen Machinery Co., Ltd.
Tool	Cem ented Carbide Coting material: TiAlN rake angle: 12°, escape angle: 7° Made by Mitsubishi Materials Corporation
Machining atmosphere	Wet (Scut FS-308CZ)
Work material	JIS C3604
Material diameter D [mm]	8.50
Machining length L [mm]	47.0
Rotational speed N [rpm]	5625
Cutting speed V_C [m/min]	150
Depth of cut t [mm]	1.30
Feed rate F [mm/rev]	0.045
Frequency f_v [Hz]	20.8–46.9
Spindle rotation per vibration E	2.0, 2.5, 3.0, 3.5, 4.0, 4.5
Spindle rotation during retract R	0.5, 0.6, 0.7, 0.8, 0.9, 1.0

3.2. Cutting Conditions

The experimental conditions are listed in **Table 2**. In this experiment, a test to change argument E was conducted using six conditions, namely setting argument E in increments of 0.5 from 2.0 (the minimum value) to 4.5 (the maximum value that can be set without changing the cutting speed). In the test to change argument R, it was changed from 0.5, the minimum value that could be set to the maximum value of 1.0, in increments of 0.1.

4. Vibration Parameter Change Test Results and Discussion

4.1. Results of Cutting Resistance Measurement Using Strain Gauge Method

Figure 9 shows the cutting resistance during 0.1 seconds of conventional cutting. The principal cutting and feed forces during conventional cutting show steady-state conditions. This is because continuous cutting was performed while maintaining a constant feed rate during conventional cutting.

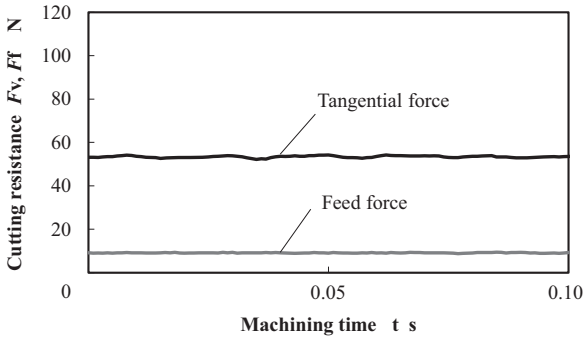

Fig. 9. Cutting resistance during conventional cutting.

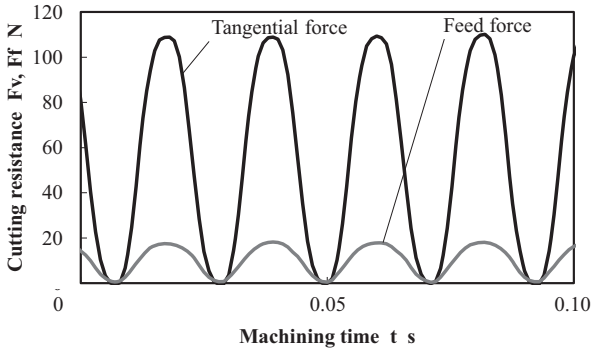

(a) $E = 2.0$, $R = 1.0$

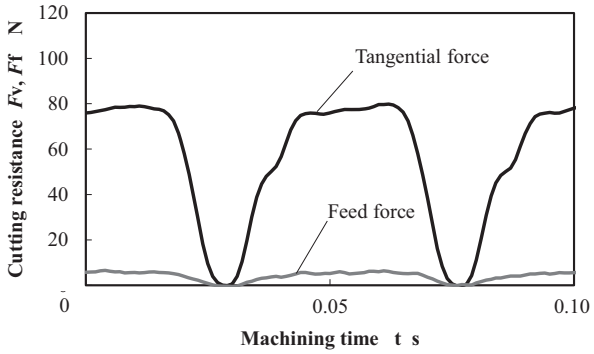

(b) $E = 4.5$, $R = 1.0$

Fig. 10. Cutting resistance in low-frequency vibration cutting.

The cutting resistance during low-frequency vibration cutting is shown in **Fig. 10**. It can be seen that the primary cutting force and feed force under the conditions of $E = 2.0$ and $R = 1.0$, as shown in **Fig. 10(a)**, fluctuate periodically owing to the effect of low-frequency vibration. The vibration frequency under these conditions is 46.9 Hz, and the cutting resistance in **Fig. 10(a)** shows an oscillation behavior of approximately 4.5 times per 0.1 seconds, which is consistent with the vibration frequency. The minimum cutting resistance was close to 0 N for both the primary cutting force and feed force, which is considered to be due to the fact that the tool and workpiece do not interfere with each other in the idle region that is characteristic of low-frequency vibration cutting.

Conversely, the peak values of the primary cutting force

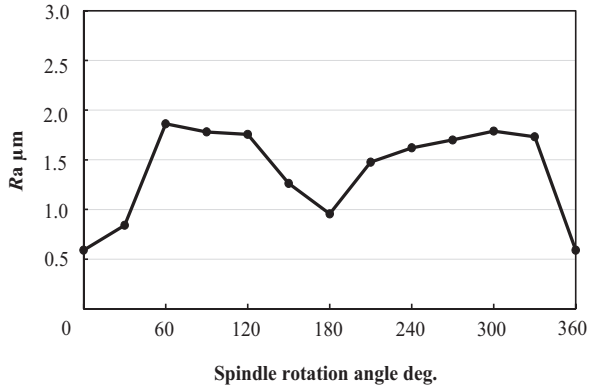

Fig. 11. Comparison of vibration behavior and surface roughness ($E = 2.0$, $R = 1.0$).

and feed force were large compared to the steady-state values in conventional cutting. This is because the cutting resistance depends on the cutting cross-section [18], and the cutting area is characterized by constant fluctuations during low-frequency vibration cutting. Because the cutting cross-section is larger at the moment of maximum feed than during conventional cutting, the load on the tool at that time is also considered to be larger. As shown in **Figs. 9** and **10(a)**, the maximum value of the cutting resistance obtained during low-frequency vibration cutting is approximately twice that obtained using conventional cutting. In this case, the resistance is almost the same as that obtained using conventional cutting. Therefore, the cutting temperature generated at the cutting edge during low-frequency vibration cutting in mode 2, which was verified in this study, was on average the same as that generated during conventional cutting.

Figure 10(b) shows the cutting resistance measurement results for $E = 4.5$ and $R = 1.0$. As in **Fig. 10(a)**, the cutting resistance fluctuates owing to the vibration behavior. The vibration frequency under this condition is 20.8 Hz, and the waveform of the cutting resistance shows approximately two vibrations, which is consistent with the vibration frequency. The peak value is smaller than that for $E = 2.0$ and $R = 1.0$. This result is thought to be due to the difference in the feed per spindle rotation shown in **Table 1**, where the feed is larger than in conventional cutting but smaller than in $E = 2.0$ and $R = 1.0$.

4.2. Results and Discussion of Workpiece Surface Properties Measurements

4.2.1. Relationship Between Surface Roughness and Vibration Behavior

Figure 11 shows the vibration behavior and transition of surface roughness measured at 12 points on the same circumference under the conditions of $E = 2.0$ and $R = 1.0$. First, it can be seen that the value of *Ra* decreases at a phase angle of 0°. This is due to the idle region indicated by the shaded line in the vibration behavior diagram, where the workpiece pre-grinding surface is evened

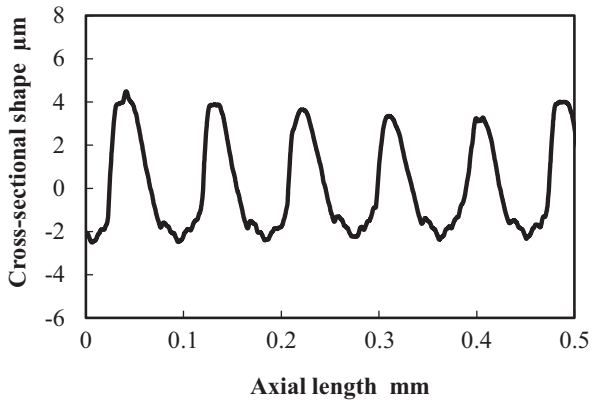

(a) *Ra* maximum phase angle (60°)

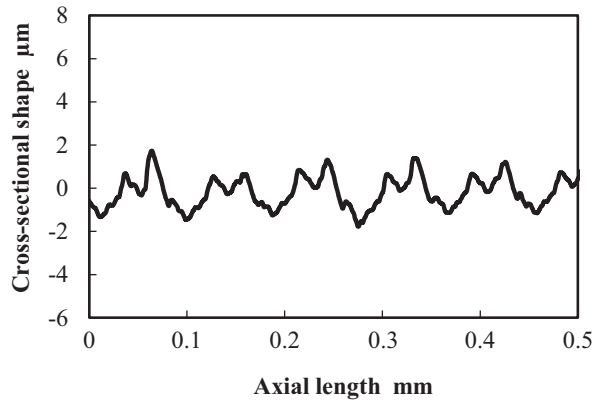

(b) *Ra* minimum phase angle (0°)

Fig. 12. Difference in cross-sectional curve by phase angle ($E = 2.0$, $R = 1.0$).

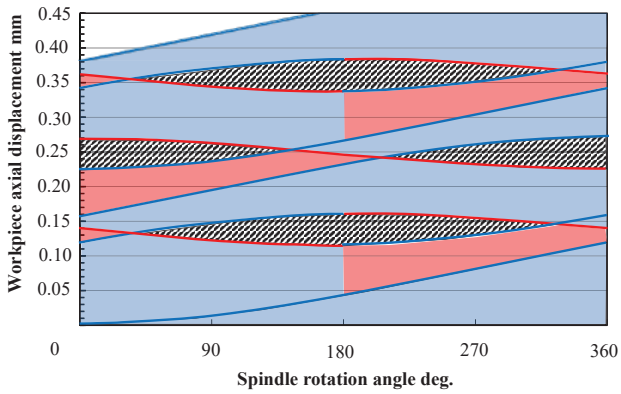

(a) Low-frequency vibration behavior

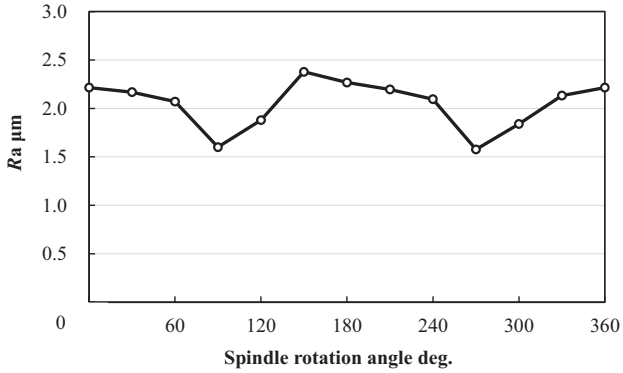

(b) Relationship between *Ra* and spindle rotation

Fig. 13. Comparison of vibration behavior and surface roughness ($E = 2.5$, $R = 1.0$).

out by the cutting edge, which suppresses the increase in surface roughness. Next, it can be confirmed that the *Ra* value increases mainly in the vicinity of 90° and 270°. This phase angle corresponds to the phase angle at which the light-blue line, indicating the cutting edge path during spindle advancement, and the red line, indicating the path during spindle retraction in the vibration behavior diagram, intersect. At this phase angle, where the cutting edge lines in the spindle advancement and in the spindle retraction intersect, the distance between the cutting edges increases, which increases the surface roughness owing to the greater unevenness formed on the cross-section. Conversely, at phase angles of 120°–240°, the cutting edges in the spindle advancement and retraction alternately form the cross-section, resulting in a smaller cutting edge spacing, which suppresses the increase in surface roughness. Thus, low-frequency vibration cutting is characterized by a constant change in the edge spacing depending on the phase angle of the workpiece, which in turn causes a change in the surface roughness.

Figure 12 shows the cross-sectional curves for $E = 2.0$ and $R = 1.0$. **Fig. 12(a)** shows the cross-sectional curve at 60°, where *Ra* is increasing. It can be confirmed that peaks and valleys are periodically formed and their pitch is consistent with 0.09 mm, which is the spindle feed for one cycle of the vibration. As mentioned above, at this phase angle, the cutting edge during the spindle advance and the cutting edge during the spindle retract overlap, and the cutting edge interval is larger than the set feed rate $f = 0.045$ mm/rev, resulting in an increase in the surface roughness. In contrast, **Fig. 12(b)** shows the cross-sectional curve at 0°, where *Ra* is the lowest among the 12 points. As in **Fig. 12(a)**, the length of one cycle of the peaks and valleys in the cross-sectional curve is 0.09 mm; however, the pitch of the peaks and valleys is 0.045 mm because two valleys are formed in one cycle, which appear to be the traces of the cutting edge. This is consistent with the feed rate $f = 0.045$ mm/rev, indicating that the surface roughness at this phase angle is equivalent to that of conventional cutting.

In low-frequency vibration cutting, the characteristics of the vibration behavior are different for integer and non-integer values of argument E. **Fig. 13** shows the vibration behavior and surface roughness transition for the non-integer value of the argument ($E = 2.5$, $R = 1.0$). Under the condition in which argument E is a non-integer, the cycle is displaced by 180° for each vibration. Therefore, the cycle of the cutting edge at the phase angle is formed with a spindle rotation equal to twice the value of argument E. In the case of $E = 2.5$, a cross-section of one cycle is formed in five rotations. As shown in **Fig. 14**, the

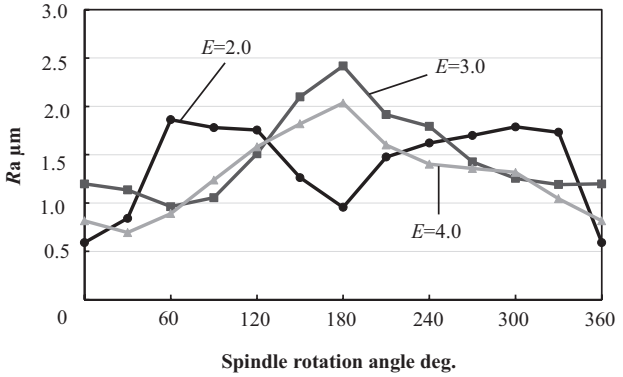

(a) E is an integer

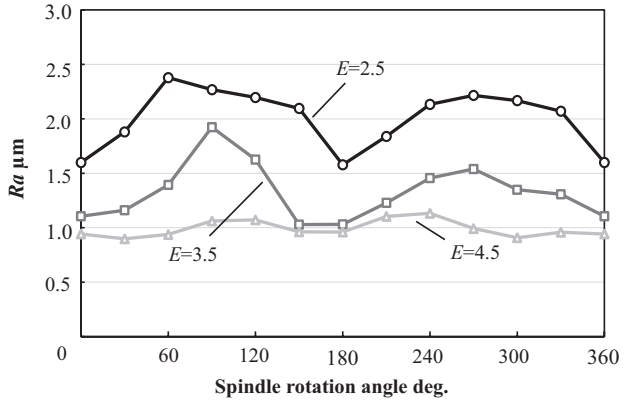

(b) E is a non-integer

Fig. 14. Transition of workpiece surface roughness due to differences in E.

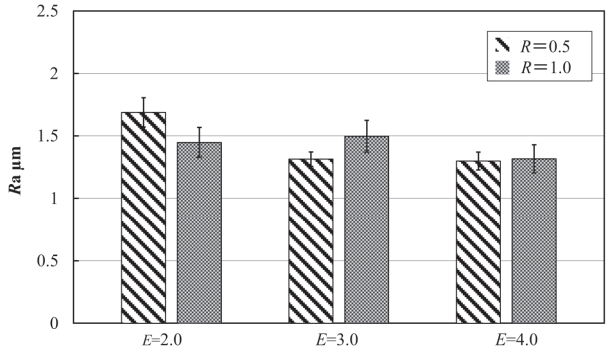

(a) E is an integer

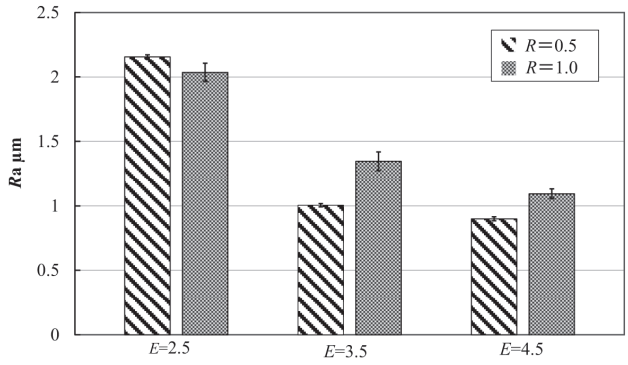

(b) E is a non-integer

Fig. 15. Surface roughness measurement results.

variation in the surface roughness increases at the phase angles (30°, 150°, 210°, and 330° in the vibration behavior diagram) where the cutting edge line during spindle advancement and that during spindle retraction cross, whereas the surface roughness decreases at phase angles of 90° and 270°, where the cutting edge lines are evenly spaced. When argument E is a non-integer, the variation in surface roughness due to differences in the phase angle is smaller than that when argument E is an integer. This is thought to be due to the fact that the shift in the vibration behavior suppresses the increase in edge interval even at the phase angles where the cutting edge lines cross between the forward and backward spindle motions.

4.2.2. Results of Workpiece Surface Roughness Measurement

Figure 14 shows the results of plotting the surface roughness of 12 workpiece points for each phase angle under each condition of argument E. **Fig. 14(a)** shows the transition of the surface roughness for the integer value of argument E. It can be seen that the values of *Ra* vary greatly with the phase angle for all conditions. The peak value of *Ra* is approximately 2–3 times higher than the lowest *Ra* value. Comparing the surface roughness at the peaks, the *Ra* value for the $E = 3.0$ condition is the largest, while the *Ra* value for the $E = 2.0$ condition is the smallest. However, under $E = 3.0$ and $E = 4.0$, the surface roughness peaks at one location, whereas under $E = 2.0$, the surface roughness increases at two phase angles. This is due to the difference in vibration behavior. As mentioned above, there is only one phase angle where the cutting edge line during spindle advancement and that during spindle retraction intersect under the conditions of $E = 3.0$ and 4.0, whereas there are two phase angles under the condition of $E = 2.0$, as shown in **Fig. 15**. Therefore, we observed two phase angles that exhibit peak values of *Ra*.

Figure 14(b) shows the transition of surface roughness under the conditions of non-integer values of argument E. As shown in **Fig. 14(b)**, the surface roughness varies depending on the phase angle. However, the range of variation is smaller than that for the integer values of argument E. In particular, the difference between the largest and smallest *Ra* values is very small, approximately 0.3 μm, for $E = 4.5$. In addition, when argument E is a non-integer, the *Ra* value tends to decrease as E increases. Especially under the condition of $E = 4.5$, the surface roughness was the best among the six conditions in this experiment, and the variation was small.

Figure 15 shows the average *Ra* and its variation for the 12 points measured for the surface roughness under each condition, with argument R set to either the minimum (0.5) or the maximum (1.0). **Fig. 15(a)** shows the results for integer values of E. As argument E increases, the average *Ra* tends to decrease, that is, the surface roughness

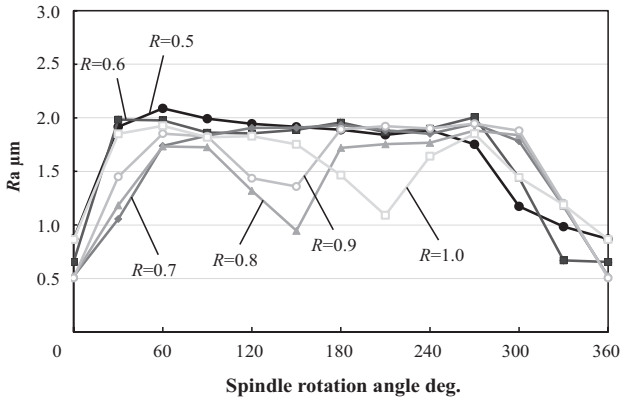

Fig. 16. Transition of workpiece surface roughness due to differences in *R*.

improves. In this section, it was mentioned that the surface roughness increases when $E = 3.0$. This is because the edge interval becomes extremely large for the $E = 3.0$ condition when different conditions are compared at the phase angle at which *Ra* reaches its maximum value. This is because the feed rate per spindle rotation is affected by the difference in vibration behavior. The feed rate listed in **Table 1** decreases as argument *E* increases. Therefore, it is considered that the average value of *Ra* is smaller under conditions where the cutting edge interval is shorter and argument *E* is larger. The variation of argument *R* is smaller when $R = 0.5$ for all conditions. The reason for this is discussed in this section.

Figure 15(b) shows the results for non-integer *E*. As in **Fig.15(a)**, the value of *Ra* tends to decrease as argument *E* increases and has a smaller variation when argument *R* is small. When argument *E* is a non-integer, the overall surface roughness variation is smaller than when *E* is an integer.

Figure 16 shows the results of the workpiece surface roughness measurements for each argument *R* when $E = 2.0$. As shown, the *Ra* values for each phase angle are plotted to examine the transition in the surface roughness. There were no significant differences in the maximum and minimum values of *Ra* for any condition. However, for *R* values of 0.5 to 0.7, the value of *Ra* was smaller at the phase angle of 0°; in contrast, for *R* values of 0.8 to 1.0, there was one more phase angle, in addition to the phase angle of 0°, where the value of *Ra* is smaller. This may be due to the difference in vibration behavior caused by changing argument *R*. From **Figs. 2(a)** and **(c)**, it can be confirmed that the idle region indicated by the shaded area is larger under conditions with large *R* values. As mentioned earlier, this idle region suppresses the increase in the surface roughness. It is considered that the surface roughness value is suppressed at the phase angle where the idle region is located because it is affected to a greater extent under the condition of a large *R* value.

These results indicate that the difference in argument *E* has a significant effect on the surface roughness of the workpiece, and that the difference in argument *R* affects the variation in surface roughness at the phase angle of the workpiece, although the effect is not as large as that of argument *E*. Argument *E* should be set to avoid integer multiples; setting it as large as possible is expected to suppress the increase in surface roughness. For argument *R*, using the smallest possible value can be expected to suppress the variation in surface roughness at each phase angle characteristic of low-frequency vibration cutting. However, it should be noted that the smaller the *R* value, the more difficult it is to break up chips.

4.3. Mechanism of Cross-Sectional Curve Formation in Low-Frequency Vibration Cutting

4.3.1. Cross-Sectional Curve Measurement Results

Figure 17 shows the cross-sectional curves at the phase angles with the maximum and minimum *Ra* values for workpieces machined under integer values of *E*. **Fig. 18** shows an example of the 3D profile under each vibration condition measured using a scanning white light interferometer (Zygo: NewView 7300). The lengths of the peaks and valleys are equal to the value of argument *E* multiplied by the set feed rate $f = 0.045$ mm/rev. This implies that the same machining phenomenon is repeated for each oscillation of the vibration behavior, which is a cutting characteristic of low-frequency vibration cutting. However, the phase angles of the maximum and minimum surface roughness for conditions of $E = 2.0$, 3.0, and 4.0 show significantly different cross-sectional curves. The cross-sectional curve for the phase angle with minimum *Ra* at $E = 2.0$ and 3.0 has twice the number of edge traces and half the pitch, because another edge trace is seen in the center of each peak, collapsing the peak. The oscillation amplitude of the cross-sectional curve is reduced because the edge traces are seen on the highest peaks of the phase angle with the maximum *Ra* even when $E = 4.0$. The number of times that the cutting edge is transferred to the cross-section of the workpiece machined using low-frequency vibration cutting increases for different phase angles, and the phase angle at which *Ra* is minimized further evens out the interval, which is thought to cause this change in the cross-sectional curve.

Figure 19 shows the cross-sectional curves of each workpiece under non-integer *E* conditions, it can be seen from the cross-sectional curves that the length curve is twice as long as the value obtained by multiplying argument *E* by the feed rate under all conditions. This implies that under the non-integer argument *E*, the machining phenomenon at the same phase angle is repeated every two vibrations because the vibration behavior is displaced by 180° in each vibration. Comparing the cross-sectional curves of the phase angles with the maximum and minimum *Ra* values for each condition, it can be seen that the pitch of the cutting edge trace is similar for each condition; however, there is a difference in the cutting edge cut depth. This difference is especially noticeable for $E = 2.5$ and 3.5. When $E = 4.5$, both **Figs. 19(e)** and **(f)** show similar cross-sectional curves in terms of the edge inter-

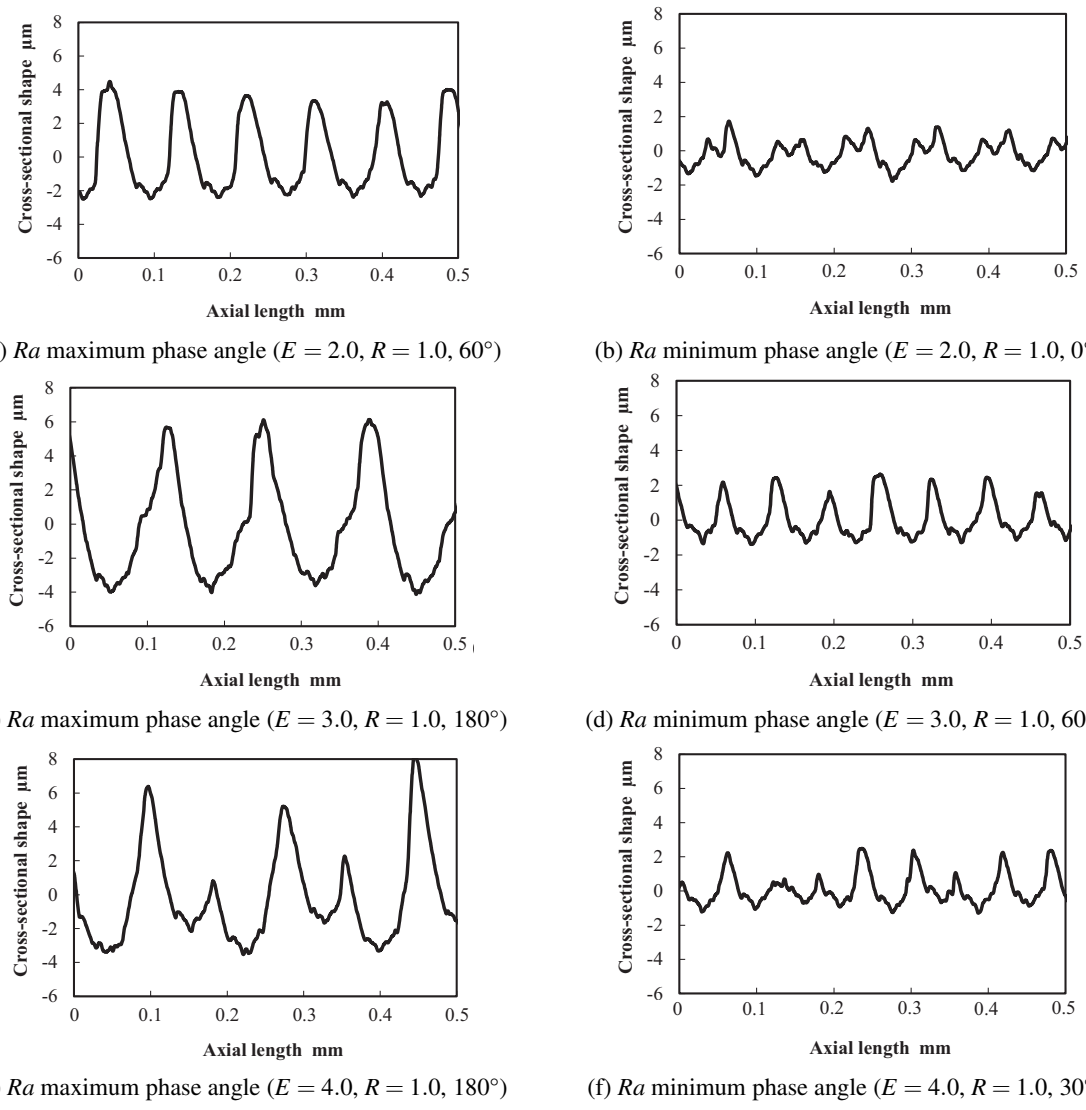

(a) *Ra* maximum phase angle ($E = 2.0$, $R = 1.0$, 60°)

(b) *Ra* minimum phase angle ($E = 2.0$, $R = 1.0$, 0°)

(c) *Ra* maximum phase angle ($E = 3.0$, $R = 1.0$, 180°)

(d) *Ra* minimum phase angle ($E = 3.0$, $R = 1.0$, 60°)

(e) *Ra* maximum phase angle ($E = 4.0$, $R = 1.0$, 180°)

(f) *Ra* minimum phase angle ($E = 4.0$, $R = 1.0$, 30°)

Fig. 17. Comparison of cross-sectional curves with integer multiples of E.

val and oscillation amplitude, indicating that the variation in surface roughness is small.

4.3.2. Relationship Between Workpiece Feed Rate and Depth of Cut

As shown in **Figs. 17(e)** and **19(a)**, **(b)**, and **(d)** in the previous section, the depth of cut fluctuated for workpieces machined under specific conditions of low-frequency vibration cutting. The cause of this phenomenon was examined by focusing on changes in the feed rate in the vibration behavior of low-frequency vibration cutting. As indicated by the curved path of the cutting edge in the vibration behavior diagram in **Fig. 1**, the feed rate constantly changes during machining during low-frequency vibration cutting. In particular, the feed rate is instantaneously zero at the phase angle at which the spindle feed switches from a forward trajectory to a backward trajectory, and the feed rate is considered to be small at the phase angles around this point. The following experiments were conducted to clarify the effect of such changes in feed rate on the depth of cut of the workpiece.

Figure 20 shows a schematic of the experiment, in which the feed rate was changed during the conventional cutting of one workpiece. The conditions for increasing the feed rate stepwise during machining are expressed in ①. The workpiece is cut at a feed rate of $f = 0.03$ mm/rev from the start of machining to an arbitrary point, and then the feed rate is changed to $f = 0.06$ mm/rev from that point. After cutting a certain distance from that point, the feed rate is further increased, and cutting is performed at a feed rate of $f = 0.09$ mm/rev until the end of machining. When the feed speed changes, there is a pause of 0.5 seconds (at a feed rate of 0 mm/rev) before switching to the next speed because of the characteristics of the machining program. In contrast to condition ①, condition ② shows a stepwise decrease in the feed rate. Under condition ③, the feed rate is constant; however, the effect of this condition was investigated by creating a pause period during machining. Machining was performed using these

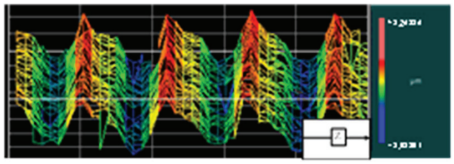

(a) $E = 2.0$, $R = 1.0$, 60°

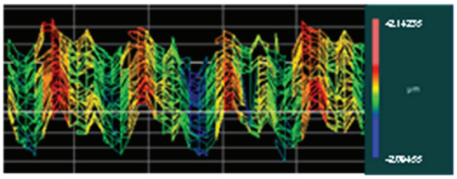

(b) $E = 2.0$, $R = 1.0$, 0°

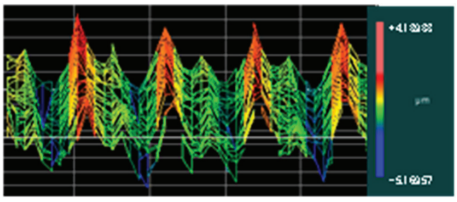

(c) $E = 4.0$, $R = 1.0$, 180°

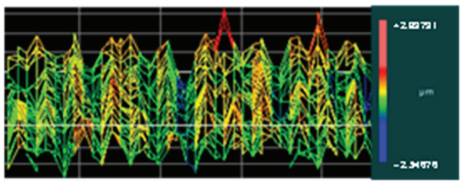

(d) $E = 4.0$, $R = 1.0$, 30°

Fig. 18. Measurement example of 3D cross-sectional curves with integer multiples of E.

three conditions, and the effect of feed rate variation was examined by examining the cross-sectional curves of the workpieces.

Figure 21 shows the results of the feed rate change tests. **Figs. 21(a)** and **(b)** show the results of cross-sectional curve measurements over the distance of 1.0 mm including the speed change point on a workpiece machined using condition ①, in which the feed rate is increased in steps. In **Fig. 21(a)**, it can be seen that the cutting depth is 1.0 to 2.0 μm deeper after the feed rate change than before the change. In **Fig. 21(b)**, the cutting depth is further increased by about 2.0 μm. In addition, the cutting depth temporarily became shallower at the feed stop point for the change of the feed rate. The same is true for the results for condition ② as indicated by **Figs. 21(c)** and **(d)**. The results show that the depth of the cut becomes deeper when the feed rate is large, and the depth of the cut becomes shallower when the feed rate changes to a small value. In the cross-sectional curve shown in **Fig. 21(e)**, it can be confirmed that the cutting depth temporarily became shallower at around 0.4 mm. This is considered to be the point where the feed was stationary, and the depth of cut became shallower because the feed rate was 0.

The above results indicate that the depth of cut of the cross-sectional curve of the workpiece is affected by changes in the feed rate, and that the greater the feed rate, the deeper the cut. In other words, the change in the cutting depth under certain conditions in low-frequency vibration cutting is thought to be influenced by the difference in the feed rate during cutting [19]. The cause of the increase in the cutting depth due to the feed rate changes is thought to be the combined effects of the shape and material of the chips and the rigidity of the machine, which causes the tool to be caught in the workpiece [20]. In mode 2, the acceleration/deceleration gradient when the tool tip vibrates is steeper than that in general-purpose cutting and mode 1; therefore, the instantaneous feed rate becomes faster than the set feed rate. Therefore, the work material is considered to undergo thermal expansion owing to the influence of the cutting temperature generated by the high feed rate on soft materials, such as free-cutting brass. The linear expansion coefficient (thermal expansion coefficient) of the free-cutting brass (JIS C3602) used in this verification experiment was 20.5×10^{-6} 1/K [21]. Because the linear expansion coefficient of general structural carbon steel is 11.8×10^{-6} 1/K [21], it is likely to be affected by thermal expansion due to the cutting temperature. Considering the physical properties of JIS C3604 and the shape of the work material, the outer diameter expands by about 3.0 μm with a temperature change of about 25°C. Similar verifications have not been performed for other work materials; however, for mode 2, there is a possibility that the depth of the cut will change in the same way for structural carbon steel. In addition, when the rake angle of the tool is large, it is considered that the depth of cut also changes because the tool is pulled in during cutting. Therefore, it is speculated that the phenomenon in which the depth of cut changes can generally occur.

4.3.3. Visualization of Cross-Sectional Curve Formation Mechanism

Considering the effects described in Section 4.3.2, the mechanism of the cross-sectional curves formed from the low-frequency vibration behavior is discussed. In **Fig. 22**, the cross-sectional curve for $E = 4.0$ and $R = 1.0$ shown by the vibration behavior is described. In this vibration behavior, the spindle rotates forward three times and then rotates backward once. The mechanism of the cross-sectional curve formation was investigated for a phase angle of 180° in the vibration behavior diagram, which is considered to increase the surface roughness the most.

Figure 23 shows the cross-sectional curve formation process. First, the first rotation in the vibration behavior, as indicated by the red plot at the bottom of **Fig. 22**, is shown in **Fig. 23(a)**. At this point, the tool tip trace, indicated by the blue object, is transferred to the workpiece. The machining conditions up to the third rotation of the vibration behavior are shown in **Fig. 23(b)**. After the tool tip of the first rotation passes, the tip trace of the second rotation is transferred at a phase angle of 180°, where the workpiece is fed by 0.08 mm, as shown in **Fig. 22**. As the third rotation is also in the spindle advance trajectory,

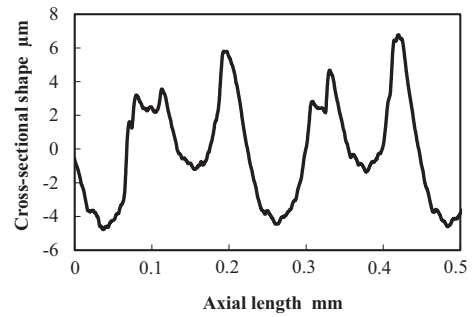

(a) *Ra* maximum phase angle ($E = 2.5$, $R = 1.0$, 60°)

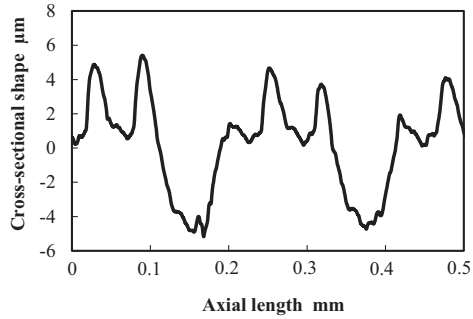

(b) *Ra* minimum phase angle ($E = 2.5$, $R = 1.0$, 0°)

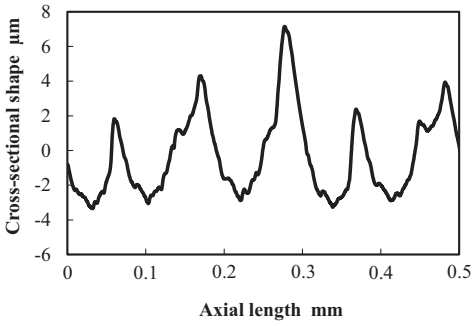

(c) *Ra* maximum phase angle ($E = 3.5$, $R = 1.0$, 90°)

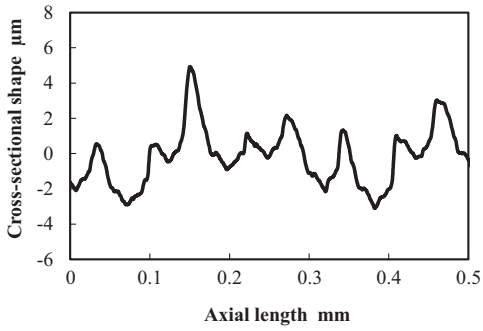

(d) *Ra* minimum phase angle ($E = 3.5$, $R = 1.0$, 180°)

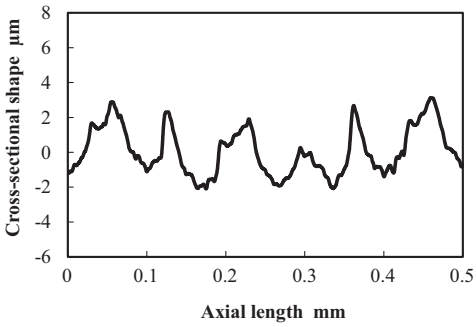

(e) *Ra* maximum phase angle ($E = 4.5$, $R = 1.0$, 120°)

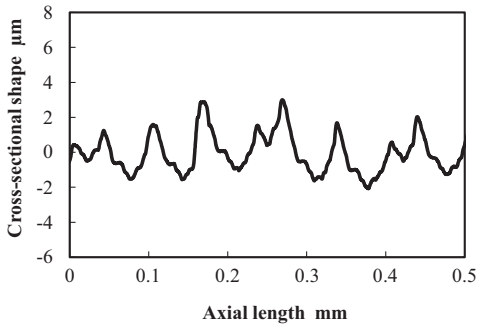

(f) *Ra* minimum phase angle ($E = 4.5$, $R = 1.0$, 30°)

Fig. 19. Comparison of cross-sectional curves with non-integer multiples of E.

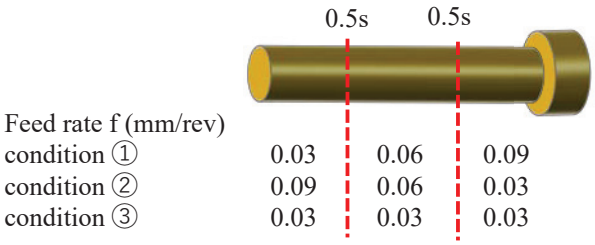

Fig. 20. Feed rate change test (Conventional cutting).

the cutting edge of the third rotation passes through after the work is fed by 0.08 mm in the same manner. The gradual deepening of the cutting depth in **Fig. 23(b)** considers the phenomenon of the tool being caught toward the workpiece, as described in Section 4.3.2. Next, **Fig. 23(c)** shows the state of the workpiece after one vibration. After the spindle moves forward with three rotations, the cutting edge passes in the spindle retraction with the fourth rotation. The cutting edge is indicated as a pink object. The tool is caught as the spindle advances; however, when the spindle retracts, the tool and workpiece are free from interference, and the tool-catching force is released immediately. Then, the cutting depth of the cutting edge trace during spindle retraction rapidly becomes shallower. The cross-sectional curve formed by the repetition of this vibration behavior is shown in **Fig. 23(d)**. The solid red line indicates the transfer mark of the cutting edge, which is formed as a cross-sectional curve. The values corresponding to the cutting edge interval in the vibration behavior diagram are shown in the figure. A comparison of the cutting edge interval with the interval between the peaks and valleys of the cross-sectional curve obtained from actual measurements confirms that the two values are almost identical. Similar results were obtained for different cut depths. The cross-sectional curve formed from the vibration behavior diagram could be predicted by considering the effect of the vibration behavior on the surface properties of the workpiece.

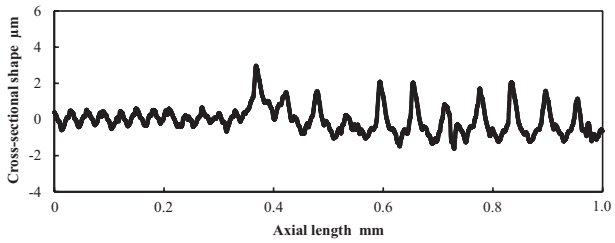

(a) Feed rate $f = 0.03$ mm/rev $\rightarrow f = 0.06$ mm/rev (condition ①)

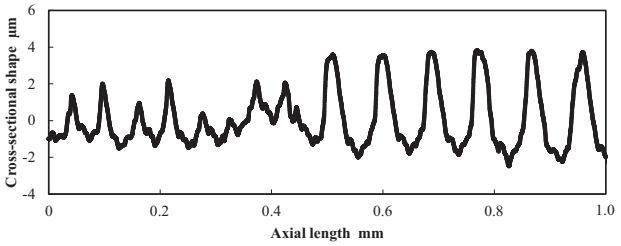

(b) Feed rate $f = 0.06$ mm/rev $\rightarrow f = 0.09$ mm/rev (condition ①)

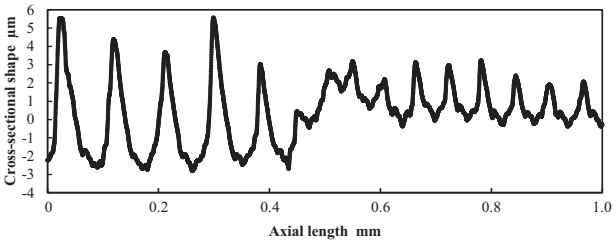

(c) Feed rate $f = 0.09$ mm/rev $\rightarrow f = 0.06$ mm/rev (condition ②)

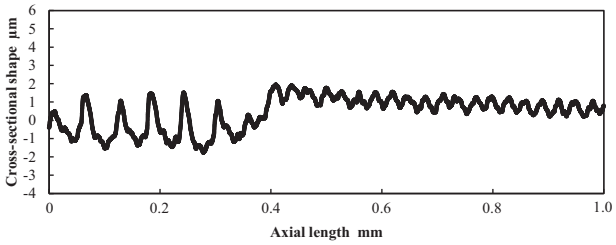

(d) Feed rate $f = 0.06$ mm/rev $\rightarrow f = 0.03$ mm/rev (condition ②)

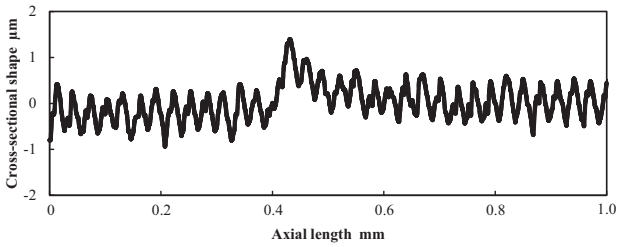

(e) Feed rate $f = 0.03$ mm/rev $\rightarrow f = 0.03$ mm/rev (condition ③)

Fig. 21. Feed rate change test cross-sectional curve measurement results.

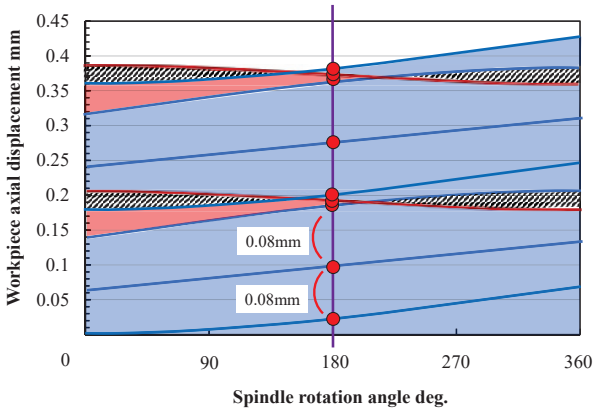

Fig. 22. Estimation of cutting edge spacing from vibration behavior diagram ($E = 4.0$, $R = 1.0$).

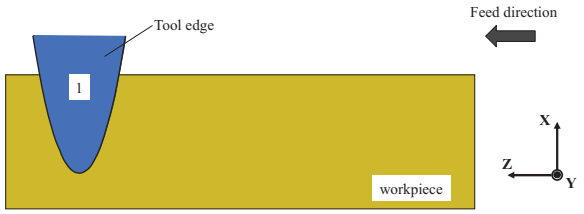

(a) At the start of cutting

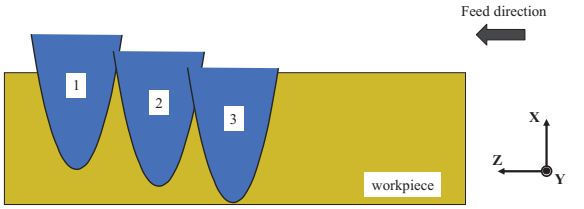

(b) At the end of the tool advancement

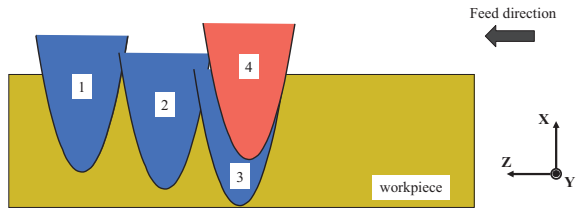

(c) At the end of one vibration

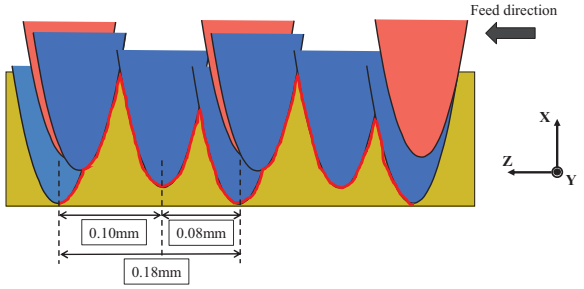

(d) After cutting

Fig. 23. Cross-sectional curve formation mechanism ($E = 4.0$, $R = 1.0$).

5. Conclusions

The objective of this study was to clarify the effect of vibration behavior on workpiece surface properties during low-frequency vibration cutting. First, the effects of the parameters that determine the vibration behavior on surface roughness were quantitatively evaluated and compared with the results of other cutting conditions. Then, we examined how the surface properties of the workpiece, such as surface roughness, roundness, and cross-sectional curves, were affected by different vibration behaviors, and, taking these results into account, we searched for optimal conditions for low-frequency vibration cutting. The main results of this study are as follows.

(1) It is preferable to set argument E, which determines low-frequency vibration behavior, to a non-integer value. Large values of E can suppress the increase in surface roughness or the variation in the phase angle. In the present study, the condition of $E = 4.5$ gives the best result for the surface roughness.

(2) Compared to argument E, argument R does not affect the surface roughness. $R = 0.5$, which is the minimum value that can be set, is expected to suppress the variation in surface roughness that arises depending on the phase-angle characteristics of low-frequency vibration cutting.

(3) In some workpieces machined under low-frequency vibration conditions, such as ($E = 2.5$, $R = 1.0$) or ($E = 3.5$, $R = 1.0$), the tool could be caught in the workpieces owing to the effect of the feed rate change during machining. This phenomenon could change the cutting depth of the workpiece and form a characteristic surface pattern on the workpiece surface.

References:

[1] A. Kitakaze, K. Noguchi, M. Muramatsu, S. Kato, K. Sannomiya, and T. Nakaya, "Development of Low Frequency Vibration-Cutting," J. of the Horological Institute of Japan, Vol.60, No.215, pp. 2-6, 2016 (in Japanese). https://doi.org/10.20805/micromechatronics.60.215_2

[2] "Cutting Tools-World Markets, End-Users & Competitors: 2005–2010," Dedalus Consulting, 2005.

[3] A. Miyake, A. Kitakaze, S. Katoh, K. Noguchi, K. Sannomiya, T. Nakaya, and H. Sasahara, "Chip control in turning with synchronization of spindle rotation and feed motion vibration," Precision Engineering, Vol.53, pp. 38-45, 2018. https://doi.org/10.1016/j.precisioneng.2018.02.012

[4] S. Ramalingam and J. D. Watson, "Tool Life Distributions–Part1: Sjngle-lnjury Tool-Life Model," Trans. ASME, J. Eng. Ind., Vol.99. No.3, pp. 519-522, 1977. https://doi.org/10.1115/1.3439271

[5] A. Miyake, H. Sasahara, A. Kitakaze, S. Katoh, M. Muramatsu, K. Noguchi, K. Sannomiya, and T. Nakaya, "Effect of Low Frequency Vibration Applied to Feed Direction on Turning Process," Int. Symp. on Flexible Automation (ISFA), pp. 356-358, 2016. https://doi.org/10.1109/ISFA.2016.7790188

[6] R. Wertheim, J. Rotberg, and A. Ber, "Influence of High-pressure Flushing through the Rake Face of the Cutting Tool," Annals of the CIRP, Vol.41, Issue 1, pp. 101-106, 1992. https://doi.org/10.1016/S0007-8506(07)61162-7

[7] I. S. Jawahir and C. A. van Luttervelt, "Recent Developments in Chip Research and Applications," CIRP Annals – Manufacturing Technology, Vol.42, No.2, pp. 659-693, 1993. https://doi.org/10.1016/S0007-8506(07)62531-1

[8] E. Shamoto and T. Moriwaki, "Ultrasonic Elliptical Vibration Cutting," CIRP Annals, Vol.44, No.1, pp. 31-34, 1995. https://doi.org/10.1016/S0007-8506(07)62269-0

[9] A. Miyake, A. Kitakaze, S. Katoh, M. Muramatsu, K. Noguchi, K. Sannomiya, T. Nakaya, and H. Sasahara, "Cutting Characteristics of Low Frequency Vibration-cutting," Proc. of JSPE, pp. 591-592, 2016 (in Japanese). https://doi.org/10.11522/pscjspe.2016A.0_591

[10] Citizen Machinery Co., Ltd., "LEV technology."https://cmj.citizen.co.jp/english/product/lfv/index.html [Accessed May 4, 2023]

[11] A. Miyake, A. Kitakaze, S. Sakurai, M. Muramatsu, K. Noguchi, K. Sannomiya, T. Nakaya, Y. Kamada, and H. Sasahara, "Influence on surface characteristics generated in Low Frequency Vibration Cutting," Trans. of the JSME, Vol.86, No.892, 2020 (in Japanese). https://doi.org/10.1299/transjsme.20-00323

[12] J. B. Mann, Y. Guo, C. Saldana, W. D. Compton, and S. Chandrasekar, "Enhancing material removal processes using modulation-assisted machining," Tribology Int., Vol.44, No.10, pp. 1225-1235, 2011. https://doi.org/10.1016/j.triboint.2011.05.023

[13] Y. Kakino, A. Matsubara, Y. Kohno, K. hloguchi, D. Murakami, and Y. Takata, "High Speed, High Productive Machining of Automobile Parts by Machining Center with High Speed and High Acceleration Rate," Proc. Third Int. Conf. Progess of Cutting and Grinding, Vol.192, 1996.

[14] Z. J. Pei, D. Prabhakar, P. M. Ferreira, and M. Haselkorn, "A mechanistic approach to the prediction of material removal rates in rotary ultrasonic machining," ASME. J. Eng. Ind., Vol.117, Issue 2, pp. 142-151, 1995. https://doi.org/10.1115/1.2803288

[15] R. Nakasawa, K. Sakai, and H. Shizuka, "The influence of additive elements on machinability of Lead free brass," Proc. of JSPE, pp. 595-596, 2016 (in Japanese). https://doi.org/10.11522/pscjspe.2016A.0_595

[16] V. Bushlya, D. Johansson, F. Lenrick, J.-E. Ståhl, and F. Schultheiss, "Wear mechanisms of uncoated and coated cemented carbide tools in machining lead-free silicon brass," Wear, Vols.376-377, Part A, pp. 143-151, 2017. https://doi.org/10.1016/j.wear.2017.01.039

[17] G. Preisinger and H. Neumater, "Brass Materials and their Application for Cages in Rolling Bearings," Tribologie und Schmierungstechnik, Vol.60, No.6, pp. 54-58, 2013.

[18] H. Kimura, T. Kitahara, and K. Mitsui, "Estimation of Cutting Force in Micro-turining," Proc. of JSPE, pp. 251-252, 2011 (in Japanese). https://doi.org/10.11522/pscjspe.2011A.0.251.0

[19] Y. Kondo, R. Hayashi, I. Yoshida, A. Kitakaza, K. Noguchi, K. Sannomiya, and T. Nakaya, "Development of Measurement and Evaluation Method for Surface Textures Manufactured by Low Frequency Vibration Cutting," Trans. of the Society of Automotive Engineers of Japan, Inc., Vol.52, No.2, pp. 407-412, 2021 (in Japanese). https://doi.org/10.11351/jsaeronbun.52.407

[20] D. Brentnall and W. Rostoker, "Some Observations on Microyielding," Acta. Met. Vol.13, Issue 3, pp. 187-198, 1965 (in Japanese). https://doi.org/10.1016/0001-6160(65)90195-1

[21] The Japan Institute of Metals and Materials, "Revised 4th Edition Metal Data Book," Maruzen Publishing, 2004 (in Japanese).

Name:
Hiroyuki Kodama

ORCID:
0000-0003-0835-4236

Affiliation:
Senior Assistant Professor, Faculty of Environmental, Life, Natural Science and Technology, Okayama University

Address:
3-1-1 Tsushima Naka, Okayama 700-8530, Japan

Brief Biographical History:
2012- Research Fellow, Japan Society for the Promotion of Science (DC2), Doshisha University
2014- Research Associate, University of Hyogo
2017- Senior Assistant Professor, Okayama University

Main Works:
• "Concentric Mutual Lapping to Improve Sliding Surface Function of SiC Ceramics," Int. J. Automation Technol., Vol.13, No.6, pp. 756-764, 2019.
• "Thermal influence on surface layer of carbon fiber reinforced plastic (CFRP) in grinding," Precision Engineering, Vol.65, pp. 53-63, 2020.
• "Abrasive jet machining for the microprofile control patterning of herringbone grooves," Precision Engineering, Vol.72, pp. 527-542, 2021.

Membership in Academic Societies:
• Japan Society of Mechanical Engineers (JSME)
• Japan Society for Precision Engineering (JSPE)
• Japan Society for Abrasive Technology (JSAT)
• International Committee for Abrasive Technology (ICAT)

Name:
Shota Matsuno

Affiliation:
Student, Graduate School of Environmental, Life, Natural Science and Technology, Okayama University

Address:
3-1-1 Tsushima Naka, Okayama 700-8530, Japan

Name:
Naoyuki Shibata

Affiliation:
Student, Graduate School of Environmental, Life, Natural Science and Technology, Okayama University

Address:
3-1-1 Tsushima Naka, Okayama 700-8530, Japan

Name:
Kazuhito Ohashi

ORCID:
0000-0001-5602-7809

Affiliation:
Professor, Faculty of Environmental, Life, Natural Science and Technology, Okayama University

Address:
3-1-1 Tsushima Naka, Okayama 700-8530, Japan

Brief Biographical History:
1989- Research Assistant, Okayama University
2004- Associate Professor, Okayama University
2016- Professor, Okayama University

Main Works:
• "Forces during Grinding Operation and its Relation to the Dressing Cycle," Advanced Materials Research, Vol.1136, pp. 78-83, 2016.
• "Thermal Influence on Surface Layer of Carbon Fiber Reinforced Plastic (CFRP) in Grinding," Precision Engineering, Vol.65, pp. 53-63, 2020.
• "Abrasive Jet Machining for the Microprofile Control Patterning of Herringbone Grooves," Precision Engineering, Vol.72, pp. 527-542, 2021.

Membership in Academic Societies:
• International Committee for Abrasive Technology (ICAT)
• Japan Society for Abrasive Technology (JSAT)
• Japan Society of Mechanical Engineers (JSME)